Shear stiffness in nanolaminar Ti_3SiC_2 challenges *ab initio* calculations

2010 J. Phys.: Condens. Matter 22 162202

(http://iopscience.iop.org/0953-8984/22/16/162202)

IOP FTC

IOP Publishing

Journal of Physics: Condensed Matter

J. Phys.: Condens. Matter **22** (2010) 162202 (5pp)

doi:10.1088/0953-8984/22/16/162202

FAST TRACK COMMUNICATION

Shear stiffness in nanolaminar Ti_3SiC_2 challenges *ab initio* calculations

E H Kisi[1], J F Zhang[1], O Kirstein[2], D P Riley[3], M J Styles[3] and A M Paradowska[4]

[1] School of Engineering, University of Newcastle, NSW 2308, Australia
[2] The Bragg Institute, ANSTO, PMB1, Menai NSW 2234, Australia
[3] Department of Mechanical Engineering, University of Melbourne, VIC 3010, Australia
[4] ISIS Neutron Scattering Facility, Rutherford Appleton Laboratory, Didcot OX11 0QX, Oxfordshire, UK

Received 19 January 2010, in final form 28 February 2010
Published 30 March 2010
Online at stacks.iop.org/JPhysCM/22/162202

Abstract

Nanolaminates such as the $M_{n+1}AX_n$ (MAX) phases are a material class with *ab initio* derived elasticity tensors published for over 250 compounds. We have for the first time experimentally determined the full elasticity tensor of the archetype MAX phase, Ti_3SiC_2, using polycrystalline samples and *in situ* neutron diffraction. The experimental elastic constants show extreme shear stiffness, with c_{44} more than five times greater than expected for an isotropic material. Such shear stiffness is quite rare in hexagonal materials and strongly contradicts the predictions of all published MAX phase elastic constants derived from *ab initio* calculations. It is concluded that second order properties such as elastic moduli derived from *ab initio* calculations require careful experimental verification. The diffraction technique used currently provides the only method of verification for the elasticity tensor for the majority of new materials where single crystals are not available.

(Some figures in this article are in colour only in the electronic version)

1. Introduction

Single crystal elastic constants are fundamental to understanding phase transitions, and a range of mechanical, fracture, wear and electro-mechanical properties. Sizeable single crystals readily yield the full elasticity tensor using ultrasonic wave speed or resonance methods. Crystals of 4–5 mm or larger are preferred although resonant ultrasound spectroscopy has made it feasible to use crystals as small as 1 mm [1]. Only the bulk elastic constants (Young's modulus, bulk modulus, shear modulus and Poisson's ratio) can be determined for materials where large single crystals cannot be grown. As a majority of new materials are not available as single crystals, there is a growing tendency to explore elastic properties through *ab initio* calculations. A class of materials to which this approach has been widely applied is the $M_{n+1}AX_n$ or MAX phases in which M is an early transition metal, A represents an A-Group element such as Si, Al, Ge, Ga, In or Sn and X is either C or N. MAX phases are of interest in a number of applications due to their interesting combination of metallic and ceramic properties [2, 3] coupled with properties unique to this material class [4]. The crystal structure of the archetype MAX phase, Ti_3SiC_2 is shown in figure 1.

MAX phase structures are hexagonal and consist of n layers of binary carbide (in this case TiC) intergrown with a single layer of the A element (in this case Si) [5, 6]. Both the layered crystal structure with long bonds between the A layer and adjacent X layers, and a tendency to fail by cleavage, led to early speculation concerning anisotropic properties [6]. As single crystals have continued to prove elusive, the physical properties have been explored using *ab initio* calculations [7–9]. Mechanical perturbation of the optimized model can supply estimates of the elasticity tensor. Such calculations have now been published for a great many MAX phases including 243 with $n = 1$ [10–16] and more than 10 with $n = 2$ or greater [14, 17–20]. In addition, calculated elastic constants have been published for related ternary carbides with more complex layered intergrowth

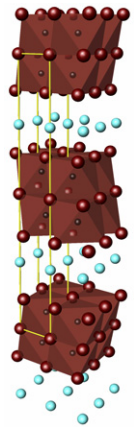

Figure 1. Clinographic view of Ti_3SiC_2 crystal structure. Note double layers of TiC octahedra interleaved by single layers of Si. The unit cell with lattice parameters $a = 3.0575$ and $c = 17.624$ Å is outlined.

structures [21]. Computed elastic constants fall into three broad categories. The first, is quasi-isotropic meaning that the following hold: $c_{11} \approx c_{33}$, $c_{12} \approx c_{13}$ and $\tau = 0.5(c_{11} - c_{13}) \approx c_{44}$. This group includes Ti_3SiC_2 [17]. In the second group, the first two conditions are met however c_{44} is slightly greater than τ—which we term slightly shear-stiff. The third group is characterized by $c_{44} < \tau$ i.e. shear-soft. All three types are illustrated in figure 2.

Elasticity tensors from *ab initio* calculations are often published at very high precision and with error estimates of equally high precision (as low as ∼0.03%), rivalling that obtainable with standard single crystal measurement techniques. Despite this apparent precision, widely different elastic constants have been published in some cases by different groups simulating the same compound. The only experimental verification for such results is agreement with the bulk elastic moduli where they are known. Unfortunately, there are infinite combinations of single crystal elastic constants that yield the same bulk elastic moduli and so a means of experimentally verifying elasticity tensors derived from *ab initio* calculations is urgently required. In this paper, we present the first experimental determination of the full elasticity tensor for a MAX phase, Ti_3SiC_2, using a solid polycrystalline sample and neutron diffraction patterns recorded from samples under *in situ* uniaxial stresses.

2. Analytical and experimental method

From shifts in the neutron diffraction peak positions, it is straightforward to measure elastic strains within crystallites having a common crystallographic vector (the scattering vector) oriented to bisect the incident and diffracted neutron beams. Many such strains, representing the average elastic response of the diffracting crystallites within the material, can be measured using a solid polycrystalline sample. In principle, the single crystal elastic constants are then available after applying a suitable tensor transformation and integrating around the scattering vector [22]. However, in polycrystals subjected to a uniaxial stress, the individual crystals experience strains that depend on a number of factors. The first of these is elastic anisotropy; an effect that is purely a function of the single crystal elastic constants. The second factor is the degree of texture (non-randomness) in the polycrystal. The third factor is the effectiveness of stress and strain transfer across grain boundaries—known as the micromechanical state [22]. To date, research relating single crystal to polycrystal elastic properties, any one of these factors may only be determined if the other two are known. In general, texture is relatively easily measured, leaving only the elasticity tensor and the micromechanical state unknown.

A new self-consistent energy balance model (SCEB) used here assumes the micromechanical state of any polycrystal to be located on the linear locus connecting states of uniform stress (Reuss limit) and uniform strain (Voigt limit). Its location is given by that point at which the microscopic strain energy density U_{int} equals the macroscopic strain energy density U_{ext}, taking into account the texture of the specimen.

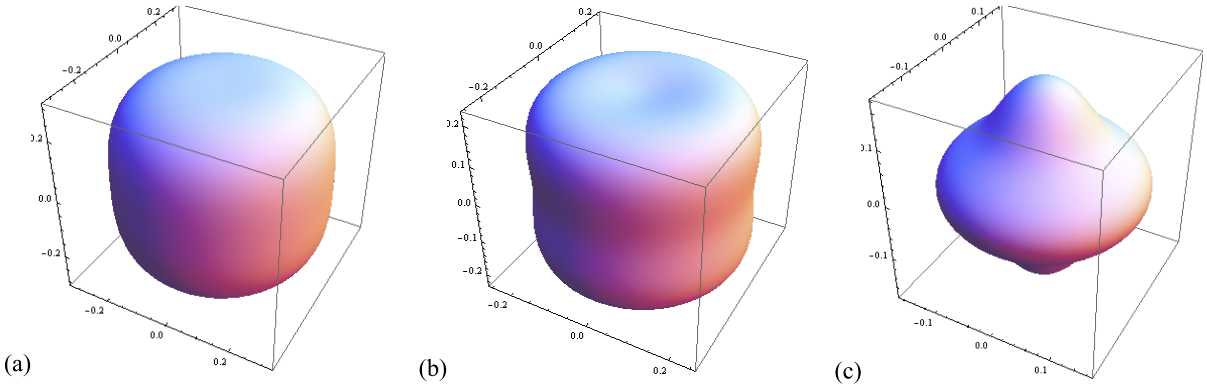

c_{11}=360, c_{12}=84, c_{13}=101, c_{33}=350, c_{44}=158

c_{11}=315, c_{12}=99, c_{13}=141, c_{33}=309, c_{44}=124

c_{11}=186, c_{12}=58, c_{13}=40, c_{33}=189, c_{44}=48

Figure 2. Typical representation surfaces for Young's modulus (E) derived from *ab initio* calculations. The distance from the origin of the figure is E in terapascal for (a) quasi-isotropic (Ti_3SiC_2) [17], (b) slightly shear-stiff (Nb_2SnC) [12] and (c) shear-soft (Sc_2AlC) [10] examples.

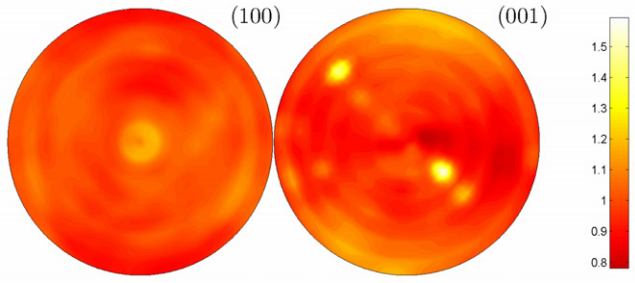

Figure 3. Pole figures of Ti_3SiC_2 for perpendicular reflections. Pole figures were calculated from the neutron diffraction determined orientation density function (ODF) [23] using data from the diffractometer KOWARI at the OPAL research reactor at ANSTO. The sample texture is effectively random as indicated by texture index $J = 1.03$ [24]. Local areas of high intensity in the 001 pole figure are due to a few large grains.

The energy balance point occurs when equation (1) is satisfied.

$$U_{\text{ext}} = \tfrac{1}{2}A_0 l_0 E\varepsilon^2 = \tfrac{1}{2}A_0 l_0 \int_0^{2\pi} E(\varphi)\varepsilon(\varphi)^2 V(\varphi)\,\mathrm{d}\varphi = U_{\text{int}}. \tag{1}$$

The macro-strain ε can be measured directly from the strain gauges and relates to the external elastic energy U_{ext} via the macroscopic Young's modulus E and the sample area A_0 and length l_0. The internal strain energy U_{int} requires knowledge of the population of different lattice planes (hkl) as a function of orientation (or texture) expressed as $V(\varphi)$, the orientation dependence of Young's modulus, $E(\varphi)$ which depends on the single crystal elasticity (compliance) tensor c_{ij} (s_{ij}), and the internal strain, $\varepsilon(\varphi)$. With this extra constraint in place, we can simultaneously determine the single crystal elastic constants *and* the micromechanical state of the polycrystal. The process is facilitated by equations for the relationship between single crystal elastic constants and strains observed during *in situ* neutron diffraction experiments under the Reuss or Voigt states [22]. For the Reuss state, equation (2) describes the relationship between the elastic compliance (ratio of strain to stress) measured parallel to the applied stress $\langle s'_{11}\rangle$, the Miller indices of the diffraction peaks hkl and lattice parameters a, b and c via $H = h/a$, $K = k/b$ and $L = l/c$. Equation (3) gives the relationship $\langle s'_{13}\rangle$ when the compliance is measured perpendicular to the applied stress.

$$\begin{aligned}\langle s'_{11}\rangle = {} & [16(H^2 + HK + K^2)^2 s_{11} + 9L^4 s_{33} \\ & + 12(H^2 + HK + K^2) \\ & \times L^2(2s_{13} + s_{44})]/(4H^2 + 4HK + 4K^2 + 3L^2)^2 \end{aligned} \tag{2}$$

$$\begin{aligned}\langle s'_{13}\rangle = {} & [6(H^2 + HK + K^2)L^2(s_{11} + s_{33} - s_{44}) \\ & + 2(H^2 + HK + K^2)(4H^2 + 4HK + 4K^2 + 3L^2)s_{12} \\ & + (8H^4 + 16H^3K - 24H^2K^2 + 16HK^3 \\ & + 8K^4 + 6H^2L^2 + 6HKL^2 \\ & + 6K^2L^2 + 9L^4)s_{13}]/(4H^2 + 4HK + 4K^2 + 3L^2)^2. \end{aligned} \tag{3}$$

For the neutron measurements, the hot-pressed polycrystalline sample with measured density of 4.175 g cm^{-3} (~92% theoretical density) was cut into a block 14.10 mm × 13.85 mm × 30.66 mm. Young's modulus was found to be 330 GPa using the longitudinal ultrasonic wave speed and Poisson's ratio has been reported in the literature to be 0.2 [2]. Optical microscopy determined the grain size in the sample to be 30–50 μm and the pores isolated. Prior neutron and x-ray diffraction analysis of the material showed no detectable amount of TiC or other common contaminant phases. A full pole figure texture measurement of this sample was completed on the instrument KOWARI at ANSTO in Sydney using 5° steps in declination (1296 data points evenly distributed in a hemi-sphere) and neutron wavelength 1.71 Å. Neutron diffraction patterns for strain determination were recorded using the time-of-flight diffractometer ENGIN-X [25] at the ISIS pulsed neutron source. The Ti_3SiC_2 sample was compressed uniaxially at stresses between 0 and 325 MPa in 25 MPa steps. Detectors located at $2\theta = \pm 90°$ and positioning the compression axis in the horizontal plane at 45° to the incident neutron beam allowed simultaneous determination of strains parallel and perpendicular to the applied stress.

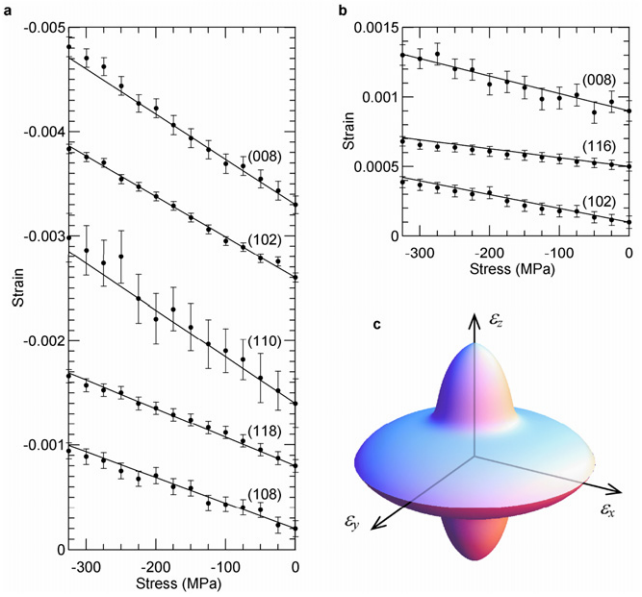

Figure 4. strain data derived from neutron diffraction experiments with *in situ* compressive stress (•). Miller indices indicate the diffracting planes. Strains are given (a) parallel and (b) perpendicular to the applied stress using a vertical offset. The solid lines represent the fit to our SCEB micromechanical model. The strain quadric derived from the experimental data is shown at (c).

3. Results and discussion

The texture results, shown in figure 3, indicate a texture index of only 1.03 (where 1 is un-textured) indicating that the sample texture may be safely ignored in our application of equations (2) and (3). A selection of strains determined from the neutron data is shown in figure 4. The elastic stiffness in crystallographic directions perpendicular to the Miller–Bravais indices shown is given by the reciprocal slope of these curves. Several general trends may be deduced directly from the raw

Table 1. Experimental elastic constants for Ti_3SiC_2 (GPa).

Model	c_{11}	c_{12}	c_{13}	c_{33}	c_{44}	$\tau = 0.5(c_{11} - c_{13})$
SCEB	279	122	122	287	440	79
Reuss	276	108	94	270	458	91
Ab initio [17]	360	84	101	350	158	130

strain data shown in figure 4 and are not model dependent. The elastic stiffness varies by a factor of two between the (0008) and $(10\bar{1}8)$ planes indicating considerable elastic anisotropy. However, in figure 4(a), the data for basal plane $11\bar{2}0$ and *c*-axis (0006 and 0008) reflections are nearly parallel illustrating near equality of c_{11} (s_{11}) and c_{33} (s_{33}). Instead, the anisotropy is in the oblique directions indicating strong shear stiffness. A detailed analysis of 24 reflections using the SCEB model quantified the anisotropy and gave the elastic constants in table 1.

Sources of error in the constants determined here centre mainly on the sample quality and the assumed micromechanical model. The sample is known to be phase pure, however it contains around 8% by volume of porosity which can be expected to make the measured elastic constants smaller than for the fully dense material. The extent of this reduction is however uncertain. Intuition suggests a linear decrease in modulus proportional to the fractional porosity for discrete pores. However, experiments on various porous ferrous alloys indicated that for small strains and comparable levels of porosity to this sample, there is no significant reduction in the Young's modulus until local plasticity at the grain corners takes place [26]. Conversely, others have reported that the modulus is reduced according to a power law in the pore fraction (see for example [27]). Based upon these precedents, we may estimate that the constants reported in table 1 may be up to 10% lower than those for the fully dense material. Possible errors introduced by the assumed micromechanical model would be a model either too Reuss-like or too Voigt-like. The Voigt model leads to isotropic elastic constants which clearly contradicts the anisotropy visible in the raw data. The elastic constants derived from a pure Reuss model are given in table 1 for comparison and contain the same essential features as those obtained from the SCEB model. Due to the energy balance constraint, the bulk average Young's modulus computed from the constants from the SCEB model in table 1 agree exactly with the value of 330 GPa measured from the ultrasonic wave speed.

Further illustration of the high shear stiffness may be seen in the Young's modulus representation surface (figure 5). Such large shear anisotropy is quite rare in hexagonal materials [28]. The shear anisotropy can be quantified by the ratio c_{44}/τ which is greater than 5.5 in this case. This is greatly at odds with other materials prone to cleavage and mechanical delamination such as graphite, the micas and MoS_2 for which this ratio is typically an order of magnitude lower than measured here for Ti_3SiC_2 [28]. In those materials, in addition to extreme shear softness, there is also strong axial anisotropy indicated by large differences between c_{11} and c_{33}.

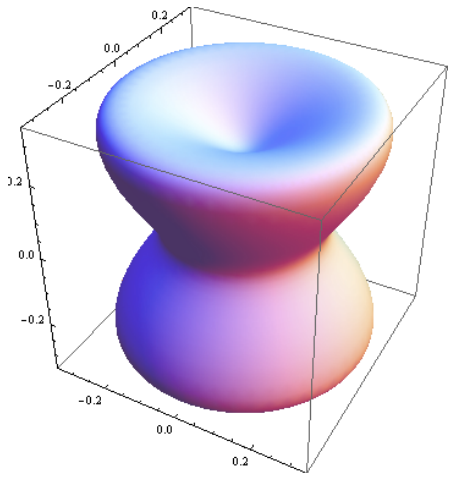

Figure 5. Representation surface for Young's modulus (E) derived from neutron diffraction data. The distance from the origin of the figure is E in terapascal to allow easy comparison with figure 2.

It is of interest to compare our results (table 1, figure 5) with typical literature values for MAX phases (figure 2) and particularly for Ti_3SiC_2 in figure 2(a). Some points of similarity are present such as the approximate equality of c_{11} and c_{33}: and values for c_{12} and c_{13} in the order of 100 GPa. However, the absolute values of the experimental constants differ greatly from the *ab initio* calculations. In particular, the computed values of c_{12} and c_{13} are 20% lower than those measured, c_{11} and c_{33} are more than 20% higher. Disagreement between *ab initio* computed elastic constants reported by different groups for the same MAX phase has been remarked upon before however the differences were seldom of this magnitude being usually smaller than 20 GPa [16]. More seriously, the computed shear modulus c_{44} is a factor of three smaller than that measured. Apart from the numerical difference, this indicates a completely different type of elastic response by the material. It therefore appears that although *ab initio* calculations routinely give sound agreement with experimentally determined bulk elastic constants for some materials, in this case prediction of the full elasticity tensor for Ti_3SiC_2 has not been successful. This finding undermines confidence in the single crystal elastic constants predicted for other MAX phases and related compounds [10–21]. Recent measurements of the electronic transport properties of Ti_2GeC_2 which indicate that predictions of those properties made by *ab initio* calculation are also incorrect add to the uncertainty [29]. Given that the major difference between theory and experiment in our case is in the shear modulus, it may be that current *ab initio* models are unable to correctly simulate the 3d orbitals of transition metals.

In addition to contributing a powerful new tool for obtaining the elasticity tensor of new materials, the SCEB model provides a framework for making experimental contact with *ab initio* results. Applying this neutron diffraction method may provide guidance to improved *ab initio* techniques capable of better reproducing experimental determinations of the anisotropic properties of materials.

Acknowledgments

Experiments at the ISIS Pulsed Neutron and Muon Source were supported by a beamtime allocation from the Science and Technology Facilities Council and funded by Australian Research Council Grant LE0882725, the Australian Access to Major Research Facilities Program (AMRFP Proposal Number 08/09-N-01) and the Australian Institute of Nuclear Science and Engineering. The texture measurement was conducted at the OPAL research reactor, (ANSTO) Sydney Australia. We thank Dr U Garbe for fruitful discussions related to the texture measurements.

References

[1] Leisure R G and Willis F A 1997 Resonant ultrasound spectroscopy *J. Phys.: Condens. Matter* **9** 6001–29
[2] Barsoum M W 2000 The MAX phases: unique new carbide and nitride materials *Prog. Solid State Chem.* **28** 201
[3] Barsoum M W and El-Raghy T 2001 The MAX phases: unique new carbide and nitride materials—ternary ceramics turn out to be surprisingly soft and machinable, yet also heat-tolerant, strong and lightweight *Am. Sci.* **89** 334–43
[4] Yoo H I, Barsoum M W and El-Raghy T 2000 Ti_3SiC_2 has negligible thermopower *Nature* **407** 581–2
[5] Jeitschko W and Nowotny H 1967 Die Kristallstruktur von Ti_3SiC_2—ein neuer komplexcarbid-typ *Monatasch. Chem.* **98** 329–37
[6] Kisi E H, Crossley J J A, Myhra S and Barsoum M W 1998 Structure and crystal chemistry Ti_3SiC_2 *J. Phys. Chem. Solids* **59** 1437–43
[7] Sun Z and Yanchoun Z 1999 *Ab initio* calculation of titanium silicon carbide *Phys. Rev.* B **60** 1441–3
[8] Medvedeva N I, Novikov D L, Invanovsky A L, Kuznetzov M V and Freeman A J 1998 Electronic properties of Ti_3SiC_2-based solid solutions *Phys. Rev.* B **58** 16042–50
[9] Segall M D *et al* 2002 First-principles simulation: ideas, illustrations and the CASTEP code *J. Phys.: Condens. Matter* **14** 2717–44
[10] Bouhemadou B 2008 First-principles study of structural and elastic properties of Sc_2AC (A = Al, Ga, In Tl) *Solid State Commun.* **146** 175–80
[11] Bouhemadou B 2008 Calculated structural and elastic properties of M_2InC (M = Sc, Ti, V, Zr, Nb, Hf, Ta) *Mod. Phys. Lett.* B **22** 2063–76
[12] Bouhemadou B 2008 Prediction study of structural and elastic properties under pressure effect of M_2SnC (M = Ti, Zr, Nb, Hf) *Physica* B **403** 2707–13
[13] Du Y L, Sun Z M, Hashimoto H and Tian W B 2008 First-principles study on electronic structure and elastic properties of Ti_2SC *Phys. Lett.* A **372** 5220–3
[14] Cover M F, Warschkow O, Bilek M M M and McKenzie D R 2008 Elastic properties of $Ti_{n+1}AlC_n$ and $Ti_{n+1}AlN_n$ phases *Adv. Eng. Mater.* **10** 935–8
[15] Medkour Y, Roumili A, Maouche D, Louail L and Haddadi R 2009 *Ab initio* study of structural, electronic, and elastic properties of M_2SbP (M = Ti, Zr, and Hf) *Eur. Phys. J.* B **68** 193–6
[16] Cover M F, Warschkow O, Bilek M M M and McKenzie D R 2009 A comprehensive survey of M_2AX phase elastic properties *J. Phys.: Condens. Matter* **21** 305403
[17] Yu R, Zhang X F, He L L and Ye H Q 2005 Topology of charge density and elastic anisotropy of Ti_3SiC_2 polymorphs *J. Mater. Res.* **20** 1180–5
[18] Zhang H Z and Wang S Q 2007 First-principles study of Ti_3AC_2 (A = Si, Al) (001) surfaces *Acta Mater.* **55** 4645–55
[19] Wang J, Wang J, Zhou Y and Hu C 2008 Phase stability, electronic structure and mechanical properties of ternary-layered carbide Nb_4AlC_3: an *ab initio* study *Acta Mater.* **56** 1511–8
[20] Du Y L, Sun Z M, Hashimoto H and Tian W B 2008 Elastic properties of Ta_4AlC_3 studied by first principles calculations *Solid state commun.* **147** 246–9
[21] Wang J and Zhou Y 2009 Recent progress in theoretical prediction, preparation, and characterization of layered ternary transition metal carbides *Annu. Rev. Mater. Res.* **39** 415–43
[22] Howard C J and Kisi E H 1999 Measurement of single crystal elastic constants by neutron diffraction from polycrystals *J. Appl. Crystallogr.* **32** 624–33
[23] Hielscher R and Schaeben H 2008 A novel pole figure inversion method: specification of the MTEX algorithm *J. Appl. Crystallogr.* **41** 1024–37
[24] Sturken E F 1960 A generalized growth index formalism *US Atomic Energy Comm. Rept* NLCO-804 *Papers Presented at the X-ray Preferred Orientation Mtg (National Lead Company of Ohio, Nov. 1959)* ed P R Morris, pp 9–24
[25] Zhang S Y *et al* 2009 Review: high-tech composites to ancient metals *Mater. Today* **12** 78–84
[26] Straffelini G, Fontanari V and Molinari A 1999 True and apparent Young's modulus in ferrous porous alloys *Mater. Sci. Eng.* A **260** 197–202
[27] Roberts A P and Garboczi E J 2000 Elastic properties of model porous ceramics *J. Am. Ceram. Soc.* **83** 3041–8
[28] Every A G and McCurdy A K (ed) 1992 *Landolt-Börnstein Numerical Data and Functional Relationships in Science And Technology, III/29a: Second and Higher Order Elastic Constants* (Berlin: Springer)
[29] Scabarozi T H *et al* 2008 Weak electronic anisotropy in the layered nanolaminate Ti_2GeC *Solid State Commun.* **146** 498–501